

Study on Electrodeposition of Ni-W-P Alloy Coating on Q235 carbon steel from Pyrophosphate Bath and Its Corrosion Resistance

Zhaoyao Sa^{1,2}, Yongshun Liang^{1,2}, Haiyang Liu^{1,2}, Junming Guo^{1,2}, Mingwu Xiang^{1,2},
Wei Bai^{1,2,*} and Changwei Su^{1,2,3}

¹ National and Local Joint Engineering Research Center for Green Preparation Technology of Biobased Materials, Yunnan Minzu University, Kunming 650500

² Key Laboratory of Green-chemistry Materials in University of Yunnan Province, Yunnan Minzu University, Kunming 650500

³ College of Materials and Chemical Engineering, Hunan Institute of Engineering, Xiangtan 411104

*E-mail: bw369852147@qq.com

Received: 14 May 2022 / Accepted: 5 June 2022 / Published: 4 July 2022

Ni-W-P alloy coatings were prepared at 40 °C and 8 A dm⁻² current density by DC electrodeposition in pyrophosphate bath, and the coatings with nanocrystalline and amorphous structures were selected for heat treatment and performance tested. The results show that W and P are deposited into the Ni lattice in the form of solid solution, the increase of H₃PO₃ mainly promotes the deposition of W, and the microhardness of Ni-W-P alloys with nanocrystalline and amorphous structures after heat treatment is higher, all above 1100 HV, the microhardness of amorphous Ni-W-P alloy is higher, up to 1139 HV. The polarization curve of Ni-W-P alloy is shifted positively, the corrosion potential is more positive, the corrosion current density is smaller, the corrosion resistance is good, and the corrosion resistance of the alloy is improved after heat treatment. The surface of the alloy is oxidized violently at 600 °C, and the R_{ct} value of the amorphous Ni-W-P alloy increases to 47963 Ω cm², and the corrosion resistance is the best.

Keywords: pyrophosphate, Ni-W-P alloy, heat treatment, microhardness, corrosion resistance

1. INTRODUCTION

In recent years, because of the nickel-based alloys such as nickel-tungsten and nickel-phosphorus alloys have high hardness and excellent wear and corrosion resistance have been widely used in industrial fields [1,2]. Although Ni-based alloys can be used directly after being prepared by electrodeposition, however, the continuous improvement of materials such as microhardness and corrosion resistance is a prerequisite for the rapid development of industry and science and technology

[2,3], moreover, the electronic wear resistance and corrosion resistance requirements under harsh conditions such as equipment and communication technology cannot be met by traditional nickel-based alloy coatings. Therefore, the improvement of the properties of Ni-based alloys is still a hot research topic, and the commonly used methods are heat treatment and the introduction of other elements to prepare multi-element alloys [4,5]. The W element has attracted much attention because it penetrates into Ni-P coating to obtain ternary alloy materials with unique properties such as high hardness and good wear and corrosion resistance. Compared with binary alloy coatings such as Ni-P and Ni-W, Ni-W-P coatings have stronger corrosion resistance and higher hardness [6-8]. It has been widely used in military, electronics, anti-corrosion and other fields as contact materials, connector devices and electromagnetic shielding materials. In addition, the co-deposition of W can also improve the thermal stability of the Ni-P coating. Most studies use Ni-P as the matrix to study the effect of W content on the coating, and most of them use citric acid as the complexing agent [9,10]. The following problems are difficult to solve: the decomposition of the complexing agent leads to the failure of the plating solution, the decline of the coating performance and the environmental protection. In contrast, as a non-cyanide electroplating process, pyrophosphate baths have the advantages of good compositional stability, the ability to produce "smooth surface" coatings, a carbon-free composition of electrolytes, and environmental safety [11]. There are still relatively few publications on Ni-W-P coatings for pyrophosphate electroplating, in which case this study is inspired.

In this study, the pyrophosphate bath was used as the raw material, and the Ni-W-P composite coating was prepared by DC electrodeposition technology, and the effects of H_3PO_3 concentration in the bath and heat treatment temperature on the structure, micromorphology, corrosion resistance and microhardness of the coating were studied.

2. EXPERIMENT

2.1 Preparation of Ni-W-P coating

In the pyrophosphate bath, the Ni-W-P coatings were electrodeposited on the Fe (Q235 carbon steel disc), the size of the substrate is 10 mm x 2 mm.

Table 1. Bath composition and plating conditions for electrodeposited Ni-W-P alloy coatings in pyrophosphate system.

Chemicals/Parameters	Values/ g L^{-1}	Process conditions	
$\text{NiSO}_4 \cdot 6\text{H}_2\text{O}$	12	Bath temperature/ $^{\circ}\text{C}$	40
$\text{Na}_2\text{WO}_4 \cdot 2\text{H}_2\text{O}$	60		
H_3PO_4 (85%)	10	Current density/ A dm^{-2}	8
$\text{Na}_4\text{P}_2\text{O}_7 \cdot 10\text{H}_2\text{O}$	40		
$\text{NH}_3 \cdot \text{H}_2\text{O}$ (25-28%)	~20	pH	8.5-9.0
H_3PO_3	5, 10, 20, 40		
$\text{C}_4\text{H}_6\text{O}_2$	0.4		

Its composition and plating parameters are shown in Table 1. All reagents are of analytical grade, and the water solvent used is deionized water. Before deposition, the substrate was pretreated by mechanical polishing first with silicon carbide waterproof sandpaper (CW-800), followed by electrochemical degreasing in 40 g L^{-1} NaOH at a constant current density of 10 A dm^{-2} for 10 minutes, washed after and activated in 10% HCl for 10 seconds. Electrodeposition was then carried out in a 500 ml reaction cell, maintain the bath temperature at $40 \text{ }^\circ\text{C}$, and deposited for 210 minutes at a constant current density of 8 A dm^{-2} . After electrodeposition, the coating was rinsed immediately, dried and stored for later use.

The rest of the parameters remain unchanged, the crystalline structures (named M) and amorphous structures (named N) Ni-W-P alloy coatings were prepared by electrodeposition in the plating solutions with the H_3PO_3 concentration of 10 g L^{-1} and 40 g L^{-1} , respectively. The M and N alloy coatings were subsequently annealed in a muffle furnace at 200, 300, 400, 500, 600 and $700 \text{ }^\circ\text{C}$ for 2 h, followed by characterization.

2.2 Performance characterization of Ni-W-P coating

The structure of the Ni-W-P coating was analyzed with a D8 Advance X-ray diffractometer using Cu $\text{K}\alpha$ radiation at $\lambda=0.15406 \text{ nm}$ in the 2θ range of 20 to 90° , and the Debye-Scherrer formula ($d=0.89\lambda/(\beta \cos\theta)$) [12] to calculate the average grain size. EDX-8000 fluorescence spectrometer was used to analyze the chemical composition of the coating. The microscopic morphology was analyzed by the Nova 450 Scanning Electron Microscope (SEM). The microhardness was measured using the HV-1000A microhardness tester, the indentation load was set to 100 gf, the holding time was 10 s, five parallel tests are averaged to reduce errors. The samples annealed above $400 \text{ }^\circ\text{C}$ were polished with W14, W7, and W3.5 metallographic sandpaper in turn due to surface oxidation.

The electrochemical performance was tested by CS350 electrochemical workstation. The saturated calomel electrode (SCE) as reference electrode, platinum plate as auxiliary electrode and the Ni-W-P alloys as working electrode. The corrosion solution is 3.5wt.% NaCl solution, the temperature is room temperature, and the test conditions are: polarization curve: swept at 1 mV s^{-1} over a range of $\pm 250 \text{ mV}$ (vs. OCP), electrochemical impedance spectroscopy (EIS): The AC amplitude is 5 mV and the sweep range is 100 kHz to 0.01 Hz.

3. RESULTS AND DISCUSSION

3.1 Structure characterization of Ni-W-P alloy coating

Figure 1a-d shows the SEM images of Ni-W-P ternary coatings prepared by electrodeposition in 5, 10, 20, 40 g L^{-1} H_3PO_3 baths. It can be seen that when the H_3PO_3 concentration (C_P) in the plating solution is 5 g L^{-1} , the surface of the prepared Ni-W-P coating is relatively rough and has many grooves, which may be due to the electrodeposition process of the Ni-W-P coating, caused by the entanglement or escape of gas. With the increase of C_P , the coating surface becomes smooth and flat.

Figure 2a shows the XRD patterns of Ni-W-P alloys prepared by electrodeposition of different C_P . It can be seen that only diffraction peaks corresponding to pure nickel (JCPDS No: 04-0850) were observed in the prepared Ni-W-P alloy coatings, indicating that in during the electrodeposition process, P and W atoms were incorporated into the Ni lattice to form a supersaturated solid solution in which P and W are the solutes and Ni is the solvent [13]. At the same time, compared with the standard diffraction peak of pure nickel, the 2θ corresponding to the diffraction peak of Ni-W-P alloy coating is slightly shifted to a lower angle, which is attributed to the different atomic radii of Ni, W and P, and the infiltration of W and P atoms causes the lattice spacing of Ni increases, resulting in local lattice distortion and an increase in lattice constant [14]. As the C_P increased to 40 g L^{-1} , the XRD peaks of the Ni-W-P alloy coating changed to the standard steamed bread peak, indicating that the Ni-W-P coating prepared at this time had an amorphous structure.

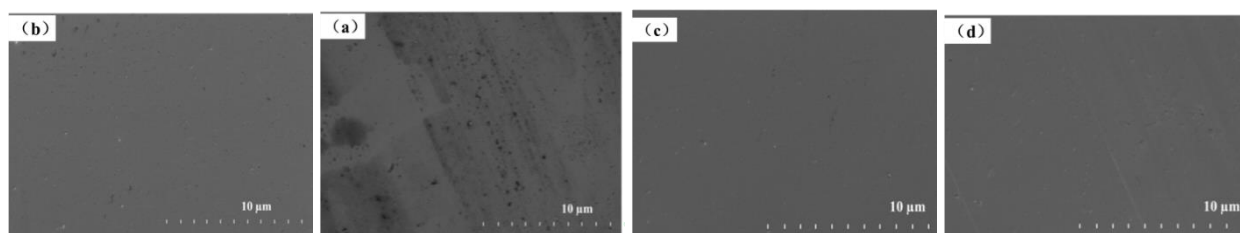


Figure 1. SEM images of Ni-W-P alloys prepared from different the H_3PO_3 concentration: (a) 5 g L^{-1} , (b) 10 g L^{-1} , (c) 20 g L^{-1} and (d) 40 g L^{-1} .

Figure 2b shows the relationship between the content of W and P elements in the coatings under different C_P . When C_P changes, the content of P in the Ni-W-P coating hardly changes, about 0.5 wt.%, but with the increase of C_P , the coating of W content in layer increases, indicating that the increase of C_P promotes the deposition of W. As the W content in the coating increases, it penetrates into the Ni lattice, and the larger atomic radius leads to the expansion of the average nearest neighbor distance of the Ni-W-P alloy, forming an amorphous structure [15].

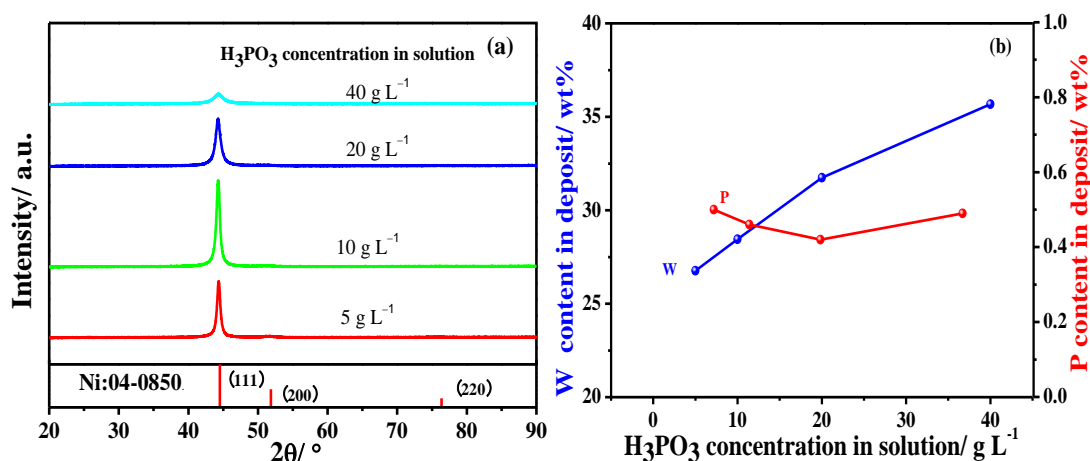


Figure 2. (a) XRD patterns of Ni-W-P coatings prepared by electrodeposition from 5, 10, 20 and 40 g L^{-1} different the H_3PO_3 concentration baths, (b) Relationship between W, P content and the H_3PO_3 concentration in Ni-W-P coating.

In order to study the effect of heat treatment on the Ni-W-P alloy coatings, the crystalline structures (named M) and amorphous structures (named N) were prepared by controlling the C_P to be 10 g L^{-1} and 40 g L^{-1} . Ni-W-P alloy coatings were annealed in a muffle furnace at 200, 300, 400, 500, 600 and 700 °C in air for 2 h, followed by characterization.

Figure 3 shows the SEM images of two Ni-W-P alloys M and N after annealing (200, 400 and 600 °C). It was observed that annealed at 200 °C, there were some micro-holes on the micro-surface of the two coatings, and there were fewer holes in N, which was due to the appearance of pores and the expansion of pits due to the escape of residual gas in the coating after heat treatment. Annealed at 400 °C, an obvious oxide layer film can be observed on the microscopic surface of the N coating. Annealed at 600 °C, as shown in Figure 3e and f, the pits on the surface of the M coating completely disappeared, and oxide particles were observed on the microscopic surface, while the thickening of the oxide layer and the oxide aggregation were observed on the surface of the N coating. The large number of needle-like small particles on the surface of the coating is caused by the growth and development of oxide particles generated by the violent oxidation of the coating, it shows that the Ni-W-P coating with amorphous structure is more easily oxidized, and the M coating with nanocrystalline structure has better oxidation resistance.

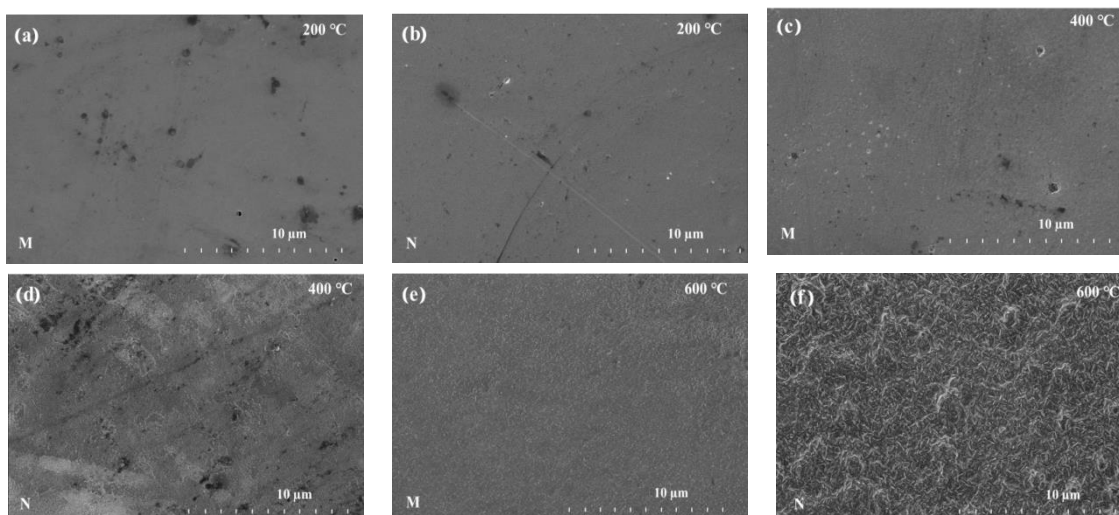


Figure 3. SEM images of the Ni-W-P alloy coatings with crystal structures (M) and amorphous structures (N) annealed at 200, 400, and 600 °C in air for 2 h.

The XRD patterns of the Ni-W-P alloys after heat treatment are shown in Figure 4. By observation, the evolution trend of XRD patterns of M and N alloys with heat treatment temperature is consistent. When the heat treatment temperature was 200 to 600 °C, as the temperature increases, the diffraction peak of the coating becomes narrower and stronger, which is caused by the crystal growth of the amorphous part of the coating. At 700 °C, the surface of the Ni-W-P alloy coating is severely oxidized to form NiWO_x oxide phase, NiO phase and Ni_3P phase, the formation of new phases destroys the crystallinity of the original Ni phase, the Ni phase decreases, and the diffraction peaks become weaker [16].

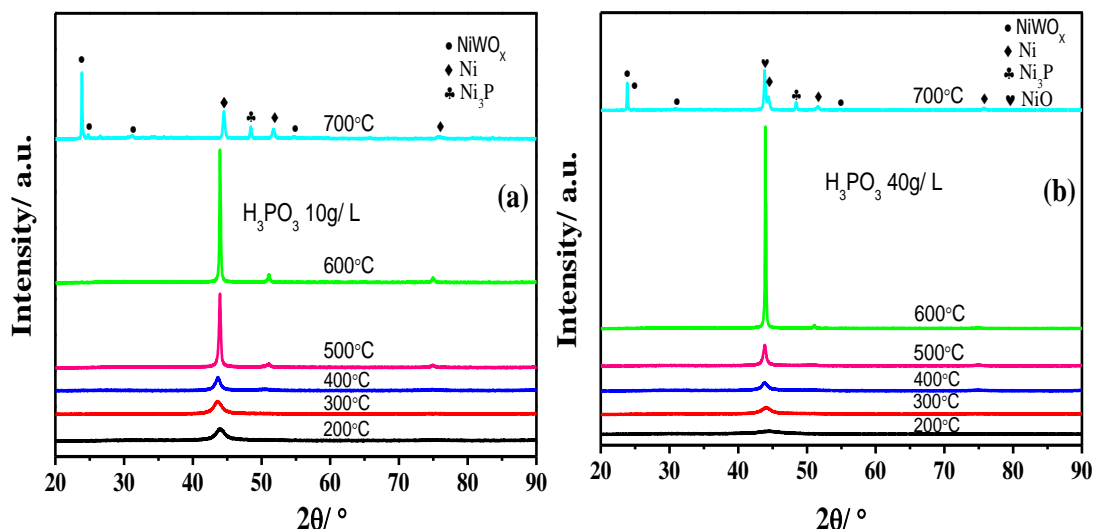


Figure 4. The XRD patterns of two structures Ni-W-P coatings annealed at different temperatures from 200 to 700 °C in air for 2 h: (a) crystal structures (M), and (b) amorphous structures (N).

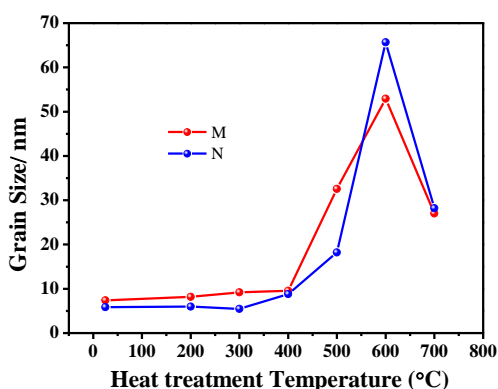


Figure 5. The Strain curves of grain size of crystalline (M) and amorphous (N) Ni-W-P alloy coatings with increasing heat treatment temperature.

Based on the XRD diffraction peaks in Figure 4, the Debye-Scherrer formula was used to calculate the grain size of the M and N alloys, the results are shown in Figure 5. The grain size of the two alloys basically did not increase below 300 °C. Above 300 °C, as the annealing temperature increases, the grain growth develops and the grain size of the alloy increases [16]. At 700 °C, due to the serious oxidation of the surface of the alloy, the precipitation of new phases leads to the reduction of the grain size of the alloy [17].

Figure 6 shows the strain curves of the microhardness of the M and N coatings with increasing heat treatment temperature. It can be seen from the figure that the microhardness of the as-deposited M and N coatings are 593 HV and 518 HV, respectively, less than 718 HV [7] value reported in the literature. This is due to the less P content in the M and N coatings and less Ni-W-P crystal phase growth [18], resulting in a decrease in microhardness. As annealing proceeds, the microhardness of M and N coatings first increased and then decreased. The increase in microhardness is because the heat treatment eliminates the residual stress inside the coating, which promotes the grain refinement and growth of the coating, and the amorphous part is crystallized, the microhardness increases [19]. The microhardness of

the alloy is the highest at 400 °C, and the microhardness value of the N coating (1139 HV) is higher than that of the M (1103 HV), which is due to the higher W content in the N coating, and the increase of the W content promotes the solid solution strengthening effect [20]. The microhardness of the M and N coatings exceeded 1100 HV, similar to the findings of Balaraju and Rajam [21] and Abhijit Biswas [22]. As the heat treatment temperature continues to increase, the grains are coarsened, the solid solution strengthening effect of Ni phase and the coherent precipitation effect of P element are weakened, and the microhardness of the alloy decreases.

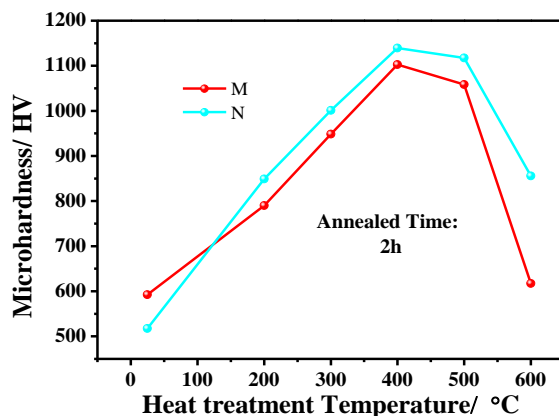


Figure 6. Microhardness curves of crystalline (M) and amorphous (N) Ni-W-P coatings annealed at different temperatures from 200 to 700 °C in air for 2h.

The corrosion resistance of Ni-W-P coatings was characterized by polarization curves and EIS in 3.5 wt.% NaCl solution. For comparison, experiments with matrix Q235 carbon steel discs (Fe) were added. Figure 7 shows the dynamic potential polarization curves of the as-deposited and annealed M and N alloys. It can be seen that after electrodepositing Ni-W-P coatings on Fe substrates, the polarization curves move up and to the left, and the corrosion potential (E_{corr}) positive shift, indicating that the corrosion resistance of the sample is improved [23], and the corrosion resistance of the M and N coating samples is better than that of the matrix Fe. This is mainly due to the passivation of the Ni-W-P coating, which produces a dense passivation film to retard corrosion [24].

The E_{corr} and corrosion current density (J_{corr}) of the M and N working electrodes were analyzed using Tafel extrapolation, and the results are shown in Table 2. The E_{corr} of the M and N coatings is more positive than that of the Fe matrix, indicating that the Ni-W-P coating is more difficult to undergo corrosion reaction in 3.5 wt.% NaCl medium [25], and as annealing proceeds, the ΔE_{corr} of the M and N coatings increases, J_{corr} decreases. This is the result that the heat treatment eliminates the residual stress caused by the side reaction of hydrogen evolution during the electrodeposition process and improves the corrosion resistance [26]. When annealed at 600 °C, the E_{corr} of the N alloy is the most positive, and the J_{corr} is the smallest, indicating that the corrosion resistance of the N coating is the best, which is the result of the more severe surface oxidation of the N coating [9].

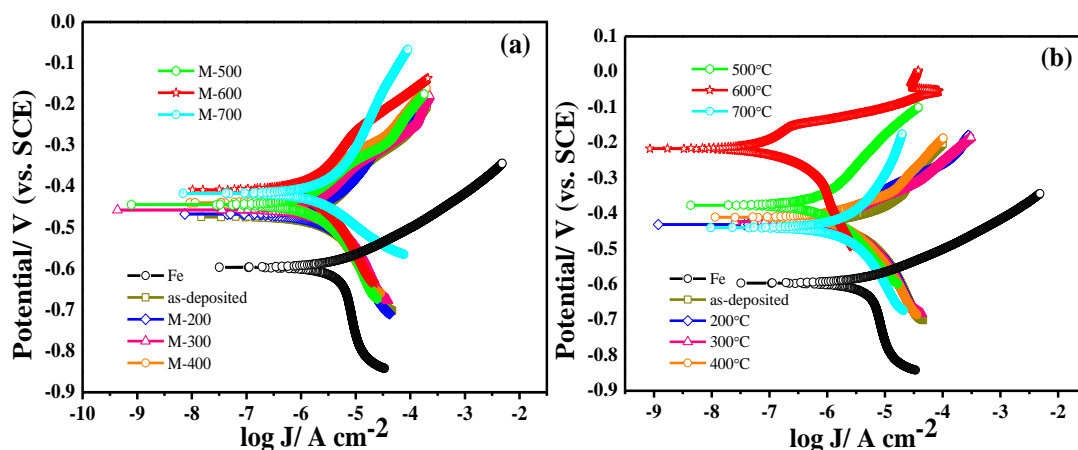


Figure 7. Polarization curves of two structures Ni-W-P alloy coatings as-deposited and annealed at different temperatures from 200 to 700 °C in air for 2 h: (a) crystalline structures (M) and (b) amorphous structures (N). Corrosive medium is 3.5 wt.% NaCl solution.

Table 2. Tafel fitting parameters of as-deposited and annealed at different temperatures from 200 to 700 °C in air for 2 h crystalline (M) and amorphous (N) Ni-W-P alloy coatings in 3.5 wt.% NaCl solution.

Sample	T/ °C	$J_{corr}/ \mu A \text{ cm}^{-2}$	E_{corr}/ mV	$\Delta E_{corr}/ \text{mV}$
Fe	-	5.71	-611	0
M	As-deposited	5.61	-473	138
	200	4.99	-460	151
	300	4.77	-468	143
	400	2.19	-431	180
	500	2.36	-444	167
	600	3.10	-409	202
	700	3.60	-416	195
N	As-deposited	8.05	-435	176
	200	3.48	-428	183
	300	2.89	-427	184
	400	2.60	-410	201
	500	2.39	-376	235
	600	0.038	-205	406
	700	5.74	-440	171

To further explore the corrosion resistance of Ni-W-P alloys, EIS tests were performed on the as-deposited and annealed M and N samples in 3.5 wt.% NaCl solution, and the Nyquist curves of the tests are shown in Figure 8. It can be seen from the figure that the semicircle sizes of the as-deposited and annealed M and N coatings are much larger than those of Fe, indicating that the Ni-W-P coatings have better corrosion resistance [27], and the equivalent circuit in Figure 8a is used to fit, the corrosion parameters of the Ni-W-P coating are shown in Table 3, where R_s , R_f , and R_{ct} are solution resistance, oxide layer resistance, and charge transfer resistance, and CPE_2 and CPE_1 are coating capacitors and electric double layer capacitors [28]. After applying Ni-W-P coating on Fe, R_{ct} increased from 895 Ω

cm² to over 10000 Ω cm², respectively, indicating that the corrosion resistance was significantly improved [29]. After heat treatment, R_{ct} further increased, and the N sample tested at 600 °C, the R_{ct} values of the M and N samples are 24791 and 47963 Ω cm², respectively. The annealed N alloy has the best corrosion resistance due to severe surface oxidation [29,30]. It is consistent with the polarization curve test results.

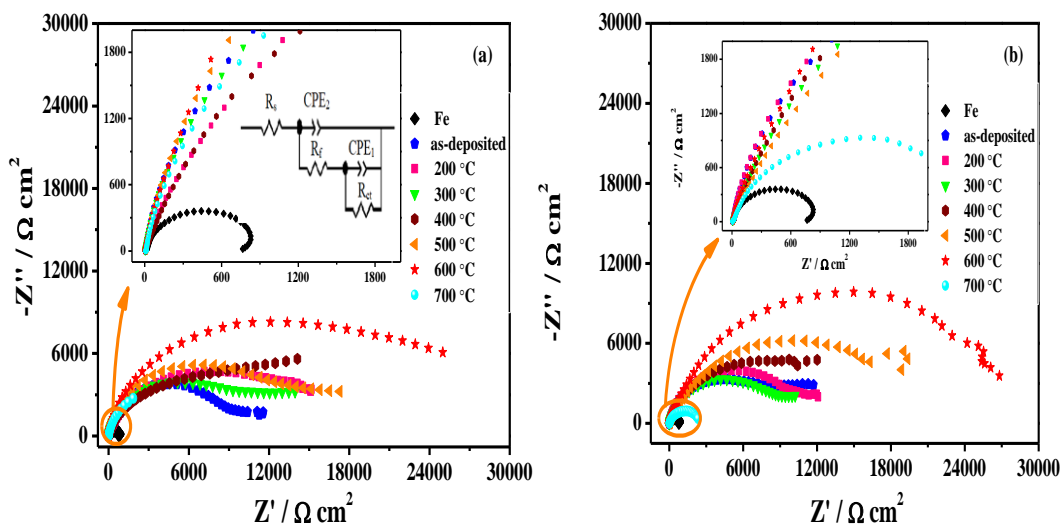


Figure 8. Nyquist curves of two structures Ni-W-P alloy coatings as-deposited and annealed at different temperatures from 200 to 700 °C in air for 2 h: (a) crystal structures (M), and (b) amorphous structures (N). Corrosive medium is 3.5 wt.% NaCl solution.

Table 3. Equivalent circuit fitting parameters of as-deposited and annealed at different temperatures from 200 to 700 °C in air for 2 h crystalline (M) and amorphous (N) Ni-W-P alloy coatings in 3.5 wt.% NaCl solution.

Sample	T/ °C	R _s / Ω cm ²	CPE ₁ -T/ F cm ⁻²	CPE ₁ -P	R _f / Ω cm ²	CPE ₂ -T/ F cm ⁻²	CPE ₂ -P	R _{ct} / Ω cm ²
Fe	-	4.44	0.00056	0.72	13.52	0.00053	0.93	895
M	-	4.69	0.000044	0.85	4.97	0.000036	1.07	10100
	200	4.15	0.000040	0.68	6.02	0.000043	1.01	15754
	300	3.12	0.000087	0.15	4.39	0.000039	0.93	11707
	400	4.28	0.00010	0.73	5.08	0.000093	1.06	18638
	500	4.53	0.000093	0.74	5.27	0.000073	1.05	15891
	600	3.82	0.000035	0.72	4.92	0.000021	0.96	24791
N	-	4.05	0.000088	0.24	3.25	0.000034	0.95	23562
	200	3.93	0.000073	0.16	1.03	0.000030	0.92	28253
	300	4.28	0.000099	0.17	0.0053	0.000051	0.88	27699
	400	5.11	0.000054	0.19	0.69	0.000089	0.81	30694
	500	4.88	0.000035	0.21	3.28	0.000054	0.79	33426
	600	4.69	0.000023	0.16	3.11	0.000023	0.83	47963

4. CONCLUSION

Ni-W-P alloy coatings were prepared by DC electrodeposition in a pyrophosphate bath, and M and N coatings with nanocrystalline and amorphous structures were heat-treated. The XRD results show that W and P are deposited into the Ni lattice in the form of solid solution. With the increase of C_P , the Ni-W-P alloy has an amorphous structure at $40 \text{ g L}^{-1} C_P$, and the EDX data shows that the increase of C_P promotes the alloy W content increased. After heat treatment, the diffraction peak of the alloy becomes stronger, the grain grows and crystallizes, and the grain size increases. Annealed at $700 \text{ }^\circ\text{C}$, new phases NiWO_x oxide phase, NiO phase, Ni phase and Ni_3P phase are formed. The microhardness of the as-deposited M and N alloys is in the range of 500-600 HV, and the microhardness is the highest at $400 \text{ }^\circ\text{C}$, both reaching above 1100 HV, showing a high microhardness. Polarization curves and EIS studies show that M and N Ni-W-P alloys have better corrosion resistance, N alloy has better corrosion resistance, E_{corr} is more positive, J_{corr} is smaller, the corrosion resistance of the alloy after heat treatment is improved, and the surface of the alloy at $600 \text{ }^\circ\text{C}$ violent oxidation, the R_{ct} values of M and N increase to 24791 and $47963 \text{ } \Omega \text{ cm}^2$, and N has the best corrosion resistance.

CONFLICTS OF INTEREST

There are no conflicts to declare.

ACKNOWLEDGEMENTS

Financial support from the Yunnan Fundamental Research Projects Youth Fund (No. 202001AU070008) and the National Natural Science Foundation of China (No. 51972282 and U1602273). We greatly acknowledge the Key Laboratory of Green-chemistry Materials at the University of Yunnan Province.

References

1. J.N. Balaraju, T.S.N. Narayanan and S.K. Sankara, *J. Appl. Electrochem.*, 33 (2003) 807-816.
2. B. Li, W. Zhang, D. Li, Y. Huan and J. Dong, *Appl. Surf. Sci.*, 458 (2018) 305-318.
3. M. Hashemi, S. Mirdamadi and H.R. Rezaie, *Electrochim. Acta*, 138 (2014) 224-231.
4. M.H. Allahyarzadeh, M. Aliofkhaeaei, A.R. Rezvanian, V. Torabinejad and A.S. Rouhaghdam, *Surf. Coat. Technol.*, 307 (2016) 978-1010.
5. H.H. Zhou, Z.W. Liao, C.X. Fang, H.X. Li, B. Feng, S. Xu, G.F. Cao and Y.F. Kuang, *Trans. Nonferrous Met. Soc. China*, 28 (2018) 88-95.
6. S.K. Tien, J.G. Duh and Y.I. Chen, *Surf. Coat. Technol.*, 177 (2004) 532-536.
7. W. Wang, X. Jü, C. Xu, W. Zhang, N. Mitsuzaki and Z. Chen, *J. Mater. Eng. Perform.*, 29 (2020) 8213-8220.
8. X. Shu, Y. Wang, X. Lu, C. Liu and W. Gao, *Surf. Coat. Technol.*, 276 (2015) 195-201.
9. Y. Gao, Z.J. Zheng, M. Zhu, and C.P. Luo, *Mater. Sci. Eng., A*, 381 (2004) 98-103.
10. M.C.L.D. Oliveira, O.V. Correa, B. Ett, I.J. Sayeg, N.B.D. Lima and R.A. Antunes, *Mater. Res.*, 21 (2017) e20170567.
11. D.V. Suvorov, G.P. Gololobov, D.Y. Tarabrin, E.V. Slivkin, S.M. Karabanov and A. Tolstoguzov, *Coatings*, 8 (2018) 233-244.
12. B. Ghorbanian, M. Tajally, S.M.M. Khoie and H. Tavakoli, *Surf. Innovations*, 8 (2020) 252-262.
13. F.J. He, Y.Z. Fang and S.J. Jin, *Wear*, 311 (2014) 14-20.
14. O. Younes, L. Zhu, Y. Rosenberg, Y. Shacham-Diamand and E. Gileadi, *Langmuir*, 17 (2001) 8270-

8275.

15. K.H. Hou, Y.F. Chang, S.M. Chang and C.M. Chang, *Thin Solid Films*, 518 (2010) 7535-7540.
16. S. Eraslan and M. Ürgen, *Surf. Coat. Technol.*, 265 (2015) 46-52.
17. C.N. Panagopoulos, G.D. Plainakis and D.A. Lagaris, *Mater. Sci. Eng., B*, 176 (2011) 477-479.
18. Y.H. Cheng, S. Cao, Q.Q. Hou, D.T. Han and Z.T. Han, *Rare Met. Mater. Eng.*, 45 (2016) 1931-1937.
19. K.H. Hou, M.C. Jeng and M.D. Ger, *J. Alloys Compd.*, 437 (2007) 289-297.
20. J.N. Balaraju, Kalavati, N.T. Manikandanath and V.W. Grips, *Surf. Coat. Technol.*, 206 (2012) 2682-2689.
21. J.N. Balaraju and K.S. Raja, *Surf. Coat. Technol.*, 195 (2005) 154-161.
22. A. Biswas, S.K. Das and P. Sahoo, *Int. Conf. Mech. Eng.*, (2018) 83-105.
23. W.S. Hwang and J.J. Lee, *Mater. Sci. Forum*, 510 (2006) 1126-1129.
24. M.G. Hosseini, M. Abdolmaleki and J. Ghahremani, *Corros. Eng. Sci. Technol.*, 49 (2014) 247-253.
25. P. Jin, C. Sun, Z. Zhang, C. Zhou and T. Williams, *Surf. Coat. Technol.*, 392 (2020) 125738.
26. H. Liu, R.X. Guo, Y. Zong, B.Q. He and L.I.U. Zhu, *Trans. Nonferrous Met. Soc. China*, 20 (2010) 1024-1031.
27. Y. Xiao, L.B. Yu, Q.J. Zhong, G.F. Gu, Q.Y. Zhou and Q.D. Zhong, *Adv. Mater. Res.*, 785 (2013) 953-956.
28. H. Luo, M. Leitch, H. Zeng and J.L. Luo, *Mater. Today Phys.*, 4 (2018) 36-42.
29. Y. Gao, Y. Wu, H. He and W. Tan, *J. Colloid Interface Sci.*, 578 (2020) 555-564.
30. L. Elias and A.C. Hegde, *Surf. Coat. Technol.*, 283 (2015) 61-69.

© 2022 The Authors. Published by ESG (www.electrochemsci.org). This article is an open access article distributed under the terms and conditions of the Creative Commons Attribution license (<http://creativecommons.org/licenses/by/4.0/>).